# Correspondence Between Energy Release Rates and Critical Shear Stresses Due to Interfacial Debonding in a Hybrid Composite


**Subham Singhamahapatra and Sivasambu Mahesh**

**Abstract** Two criteria for the propagation of a debond crack in a carbon-glass–epoxy hybrid unidirectional composite material are investigated comparatively. The first criterion is based on the fracture mechanics notion of a critical energy release rate. The second criterion is based on a critical interfacial shear stress threshold. In the case of simple microbonding test both the criteria have been shown in the literature to be consistent, i.e. a unique critical energy release rate and a unique critical shear stress threshold both characterize the debond crack propagation. Contrary to this observation, it is presently shown using finite element analysis that the two criteria predict inconsistent debond crack propagation in a hybrid composite.

**Keywords** Hybrid composite · Interfacial debonding · Energy release rates · Finite element analysis · Residual stress · Shear-lag

## 1 Introduction

Lightweight structural design has always been the keen interest in various industries, particularly in aerospace, mechanical, automobile and automotive applications for weight-sensitive applications. Fibre reinforced composites are of great interest because of their excellent strength and stiffness combined with a low density. However, the strength and stiffness of these composites are quite high but their toughness is limited. Therefore, these fibre reinforced composites face a strength versus toughness dilemma. To improve the toughness of these lightweight materials, the research interest in "hybridization" is reviving. In a hybrid composite, two or more different types of fibres are reinforced in the matrix which have typically a large

S. Singhamahapatra (✉) · S. Mahesh
Department of Aerospace Engineering, IIT Madras, Chennai, India
e-mail: subhamiitmadras@gmail.com

S. Mahesh
e-mail: smahesh@iitm.ac.in



P. Kumari and S. K. Dwivedy (eds.), *Recent Advances in Mechanics of Functional Materials and Structures*, Lecture Notes in Mechanical Engineering,
https://doi.org/10.1007/978-981-99-5919-8_40

stiffness contrast, for example, epoxy matrix reinforced by carbon and glass fibres. The main purpose of bringing such different types of fibres into a single composite is to gain the advantages of both of them and to alleviate some of the disadvantages. This fibre hybridization technique enhances the failure strains of fibre reinforced composites [1].

Failure studies of hybrid composites must account for the interfacial debonding in order to correctly represent the dominant failure mechanism [2]. Typically, the interfacial debonding is assumed to occur when the interfacial shear stress exceeds a critical threshold value in computational models. However, it is not clear whether this critical shear stress-based approach is consistent with the fracture mechanics notion of interfacial debond crack propagation based on the critical energy release rates criterion. In particular, it is not clear whether there exists a critical shear stress criterion for any normal compressive residual stresses at the interface induced during curing of composites from higher temperatures [3].

In this present work, the question on the validity of the critical shear stress criterion in governing interfacial debond crack propagation is addressed. The energy release rates associated with interfacial debond crack propagation in a carbon-glass–epoxy hybrid composite is determined using the virtual crack closure technique (VCCT) [4] and finite element analysis. The critical shear stress associated with interfacial debond crack propagation is determined from finite element discretization of a shear-lag model [5]. It is shown that the consistency between the critical shear stress-based approach and the fracture mechanics notion of interfacial debond crack propagation based on the critical energy release rates approach for a carbon-glass–epoxy hybrid composite could not be established. The validity of a critical shear stress-based criterion for interfacial debonding in computational studies of composite fracture could not be established for a carbon-glass–epoxy hybrid composite.

## 2 Models

### *2.1 Finite Element Model of a Carbon-Glass–Epoxy Hybrid Composite*

A three-dimensional (3D) finite element model of a transversely cracked unidirectional hybrid composite is shown in Fig. 1. It consists of a homogeneous linear elastic epoxy matrix reinforced by two types of infinitely long, linear elastic carbon (stiffer) and glass fibres (compliant). The fibres are arranged in an alternate fashion and are loaded in uniaxial tension, whereas the matrix elements are shear. Table 1 shows the properties of the fibres and matrix.

The length ($L$) of the model composite is calculated by first calculating the ineffective length ($\delta$) of the composite material using Eq. (1), separately for both carbon and glass fibres and then calculating the length of the composite ($L > 20\,\delta$) by taking the smaller of the two.

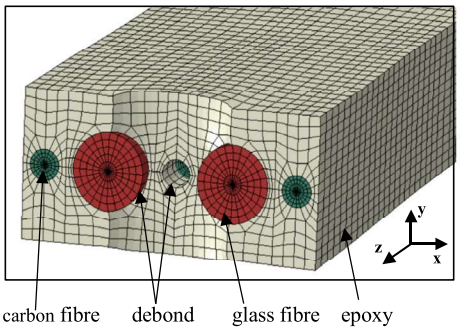


(a) Hybrid composite lamina with debonding

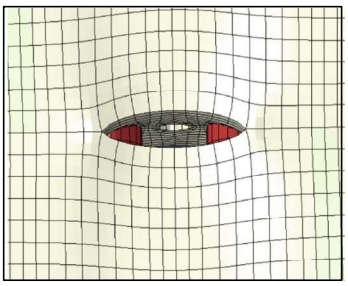

(b)Transverse crack showing debonding

**Fig. 1** (**a**) Section of 3D unidirectional hybrid composite with debonding; (**b**) with transverse crack

**Table 1** Material properties and diameters (As per Mishnaevsky 2014)

| Materials | Young's modulus, $E$ (GPa) | Poisson's ratio, $\nu$ | Coefficient of thermal expansion, $\alpha$ (/°C) | Diameter (μm) |
|---|---|---|---|---|
| Carbon | 276 | 0.37 | $0.15 \times 10^{-5}$ | 7 |
| Glass | 72 | 0.26 | $0.49 \times 10^{-5}$ | 17 |
| Epoxy | 3.79 | 0.37 | $5.4 \times 10^{-5}$ | – |

$$\delta = \sqrt{\frac{EAd_g}{GD}}, \tag{1}$$

where

$E$ Young's modulus of the fibre material
$A$ Cross-sectional area of the fibre
$d_g$ Centre to entre fibre spacing distance
$G$ Shear modulus of the material
$D$ Diameter of the bigger fibre

Equation (1) results in smaller ineffective length for carbon fibre, $\delta = 83.67$ μm and the length of the composite is chosen as, $L = 40\ \delta = 3348$ μm.

In order to simulate the compressive residual stress at interface, the finite element model is taken to be stress-free at temperatures of (a) 0 °C (b) 90 °C (c) 180 °C above the testing temperature. It is ensured that the length of the interfacial debond crack is kept well within the ineffective length of the composite and interfacial friction in the debonded region is completely neglected. The finite element model is discretized with hexagonal twenty-node solid elements with quadratic interpolation functions. To reduce the computational cost, mesh elements are biased with finer elements near the crack and coarser elements beyond. Only one-eighth of the model is simulated in order to reduce the size of the computational domain.

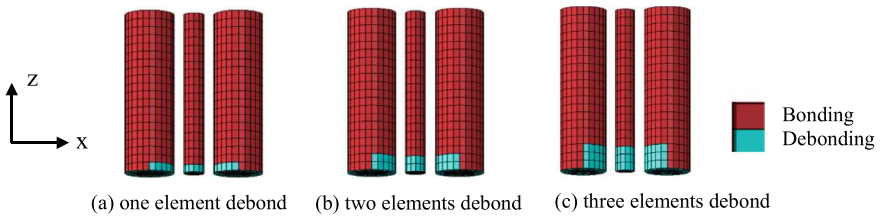


**Fig. 2** Element size-wise variation of debond crack length variation along fibre direction

Interfacial debond cracks are introduced by initially releasing the two fibre-matrix surfaces completely and are then tied together over their non-bonded lengths through tie-constraint such that there is no relative motion between the two surfaces. Moreover, equation constraints are used in the debonded region of the fibre-matrix interface along $x$- and $y$-directions so as to prevent the interpenetration of the fibre and the matrix. Starting from one element crack length, the interfacial debond crack is varied gradually by increasing the crack length after every simulation by one element size as shown in Fig. 2.

The field variables, viz. nodal forces and displacement, are measured on the glass–epoxy interface for the calculation of energy release rates. The strain energy release rates, viz. $G_1$, $G_{II}$ and $G_{III,}$ are evaluated using the modified-VCCT [4] for each interfacial debond crack length. The effect of curing from different stress-free temperatures on the energy released rates is studied and compared with shear-lag model.

## 2.2 *Shear-Lag Finite Element Model of Carbon-Glass–Epoxy Hybrid Composite*

Analytical formula for the stress state in fibre reinforced composites is usually obtained using one-dimensional (1D) shear-lag model [5, 6]. Finite element model which mimics the shear-lag model of the present composite is shown in Fig. 3a. The width of the fibre is equal to the actual diameter, whereas the height of the fibre is so chosen that the volume of the fibre remains identical with the previous full detailed model. In this model, each fibre and matrix bay cross-section is represented using one linear element. The discretization of model along the fibre direction in Fig. 3a is same as that in Fig. 1. All the elements undergo homogeneous deformation as in the shear-lag model of Hedgepeth [5].

To avoid the stress singularity at the crack tip, the glass–epoxy interface is released up to the debonded length and the shear stresses are measured on the carbon-epoxy interface for each interfacial debond crack length at the integration points. No effect on the variation of macroscopic residual stresses is studied in shear-lag model as the matrix does not carry any transverse load as per standard shear-lag assumptions [5].

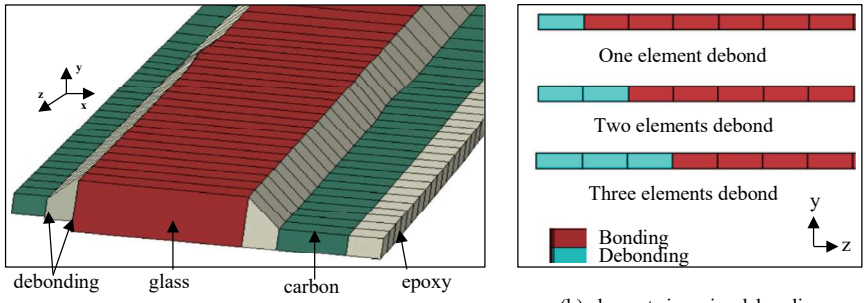


(a) shear-lag model of unidirectional hybrid composite (b) element size wise debonding

**Fig. 3** (**a**) Shear-lag model of unidirectional hybrid composite; (**b**) element size wise debonding

A comparative study of the energy release rates at different curing temperatures is made with the critical shear stress obtained from the shear-lag model.

## 3 Results

The calculation of the energy release rates for the three modes $G_{\mathrm{I}}$, $G_{\mathrm{II}}$ and $G_{\mathrm{III}}$ associated with a debond crack propagation in the composite with no residual stress is shown in Fig. 4. It is seen that $G_{\mathrm{II}} \gg G_{\mathrm{I}}, G_{\mathrm{III}}$. This is consistent with the findings of Liu and Nairn [6] for the microbond test. The decrease in $G_{\mathrm{II}}$ with the increase in debond crack length is surprising. This happens because the debond crack propagation is significantly promoted by the transverse crack at the shorter debond crack length. The $G_{\mathrm{II}}$ approaches a steady-state asymptote for a larger debond crack length. This shows that the debond crack may seize extending when $G_{\mathrm{II}} = G_{\mathrm{IIc}}$, the critical energy release rate. Because $G_{\mathrm{I}}$ and $G_{\mathrm{II}}$ are negligible, henceforth, attention will be focussed upon $G_{\mathrm{II}}$ only.

Figure 5 shows the energy release rate, $G_{\mathrm{II}}$ at three different curing temperatures. It is evident that the energy release rate at higher curing temperature is greater than that of lower temperature. It shows the great importance of residual stresses on the debond crack propagation. This is also consistent with the findings of Liu and Nairn [6].

Figure 6 shows the maximum shear stress ($\tau^*$) at the tip of debond crack length in the shear-lag model.

The energy release rate, $G_{\mathrm{II}}$ scales with the far field applied stress $\sigma_\infty$ as $G_{\mathrm{II}} \propto {\sigma_\infty}^2$, and the shear stress ($\tau$) in the shear-lag model scales as $\tau \propto \sigma_\infty$. If crack propagation were assumed to occur at constant critical energy release rate ($G_{\mathrm{IIc}}$) and constant critical shear stress ($\tau^*$), then the conditions of debond crack propagation are $G_{\mathrm{II}} = G_{\mathrm{IIc}}$ and $\tau = \tau^*$. The first of these conditions implies that

$$G_{\mathrm{II}} = G_{\mathrm{II}}(z) = G_{\mathrm{IIc}}$$

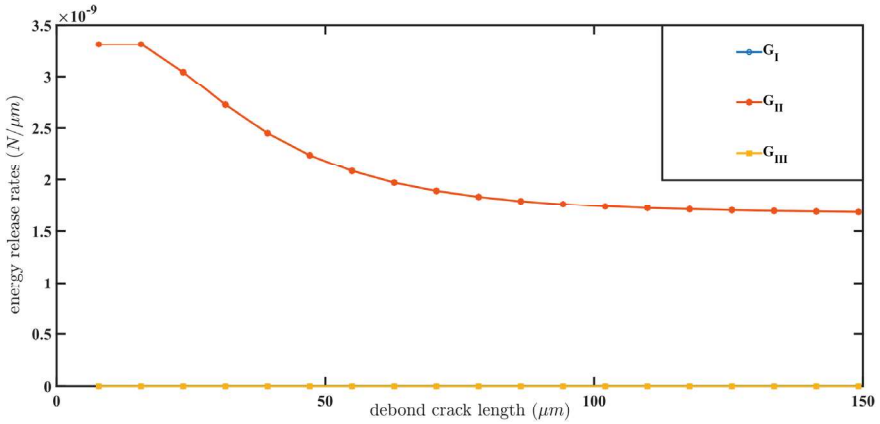


**Fig. 4** Energy release rates, $G_{\mathrm{I}}$, $G_{\mathrm{II}}$ and $G_{\mathrm{III}}$ with debond crack length without any residual stresses

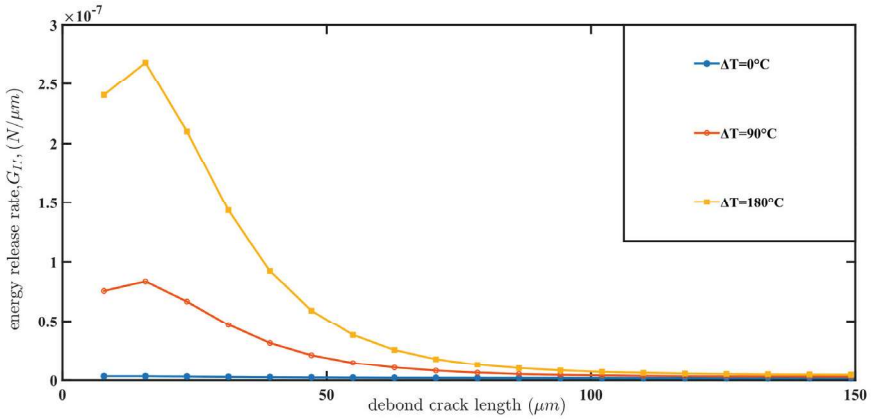


**Fig. 5** Energy release rate, $G_{\mathrm{II}}$ with debond crack length at various curing temperatures

$$
\begin{aligned}
&\Rightarrow G_{\mathrm{II}}(z) \times \frac{\sigma_\infty^2}{\sigma_{\mathrm{ref}}^2} = G_{\mathrm{IIc}} \\
&\Rightarrow \frac{\sigma_\infty}{\sigma_{\mathrm{ref}}} = \sqrt{\frac{G_{\mathrm{IIc}}}{G_{\mathrm{II}}(z)}} = \sqrt{\frac{G_{\mathrm{IIc}} \times G_{\mathrm{IIref}}}{G_{\mathrm{IIref}} \times G_{\mathrm{II}}(z)}} \\
&\Rightarrow \log\left(\frac{\sigma_\infty}{\sigma_{\mathrm{ref}}}\right) = \frac{1}{2}\left[\log\left(\frac{G_{\mathrm{IIc}}}{G_{\mathrm{IIref}}}\right) + \log\left(\frac{G_{\mathrm{IIref}}}{G_{\mathrm{II}}(z)}\right)\right] \\
&\Rightarrow \left[\log\left(\frac{\sigma_\infty}{\sigma_{\mathrm{ref}}}\right) - \frac{1}{2}\log\left(\frac{G_{\mathrm{IIc}}}{G_{\mathrm{IIref}}}\right)\right] = \frac{1}{2}\left[\log\left(\frac{G_{\mathrm{IIref}}}{G_{\mathrm{II}}(z)}\right)\right] \\
&\Rightarrow \left[\log\left(\frac{\sigma_\infty}{\sigma_{\mathrm{ref}}}\right) - \frac{1}{2}\log\left(\frac{G_{\mathrm{IIc}}}{G_{\mathrm{IIref}}}\right)\right] = \frac{1}{2}\left[\log(G_{\mathrm{IIref}}) - \log(G_{\mathrm{II}}(z))\right] \qquad (2)
\end{aligned}
$$

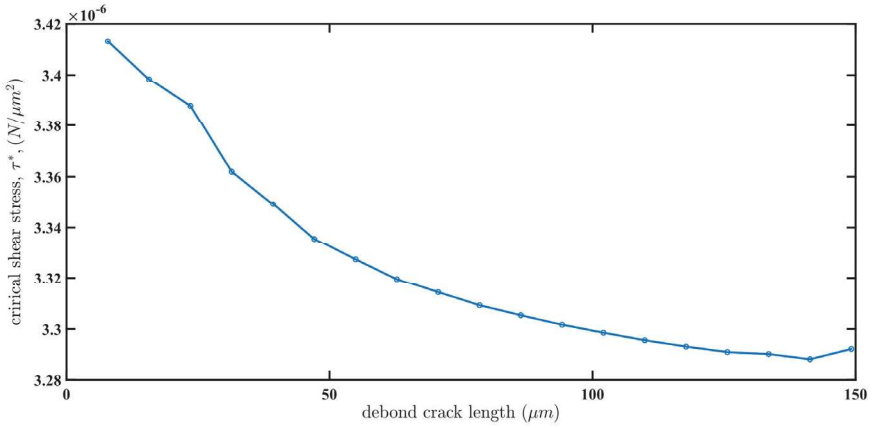


**Fig. 6** Variation of critical shear stress, $\tau^*$ at tip of debond crack in shear-lag model

Similarly, the second condition implies that

$$\begin{aligned}
&\tau = \tau(z) = \tau* \\
&\Rightarrow \frac{\sigma_\infty}{\sigma_{\text{ref}}} = \frac{\tau^*}{\tau(z)} = \frac{\tau^* \times \tau_{\text{ref}}}{\tau_{\text{ref}} \times \tau(z)} \\
&\Rightarrow \log\left(\frac{\sigma_\infty}{\sigma_{\text{ref}}}\right) = \left[\log\left(\frac{\tau^*}{\tau_{\text{ref}}}\right) + \log\left(\frac{\tau_{\text{ref}}}{\tau(z)}\right)\right] \\
&\Rightarrow \left[\log\left(\frac{\sigma_\infty}{\sigma_{\text{ref}}}\right) - \log\left(\frac{\tau^*}{\tau_{\text{ref}}}\right)\right] = \left[\log\left(\frac{\tau_{\text{ref}}}{\tau(z)}\right)\right] \\
&\Rightarrow \left[\log\left(\frac{\sigma_\infty}{\sigma_{\text{ref}}}\right) - \log\left(\frac{\tau^*}{\tau_{\text{ref}}}\right)\right] = \left[\log(\tau_{\text{ref}}) - \log(\tau(z))\right] \qquad (3)
\end{aligned}$$

Figure 7 plots the variation of $\left[-\frac{1}{2}\log(G_{\text{II}}(z))\right]$ versus the debond crack length and $\left[-\log(\tau(z))\right]$ versus the debond crack length. According to Eqs. (2) and (3), $\log\left(\frac{\sigma_\infty}{\sigma_{\text{ref}}}\right)$ can be obtained by translating these curves by $\left[\frac{1}{2}\log(G_{\text{IIc}})\right]$ and $\left[\log(\tau^*)\right]$ in the ordinate direction, respectively. If the propagation of the debond crack could be described in terms of both the energy condition, Eq. (2) and the stress condition, Eq. (3), then it should be possible to reasonably match the curves of $\left[-\frac{1}{2}\log(G_{\text{II}}(z))\right]$ versus the debond crack length and $\left[-\log(\tau(z))\right]$ versus the debond crack length by shifting them in the ordinate direction appropriately. However, it is evident from Fig. 7, that such coincidence will not occur presently, except at very large debond crack lengths.

This leads to the conclusion that the energy-based and stress-based criteria lead to inconsistent predictions of the interfacial debond crack propagation. This result is in contrary to that of Zhandarov et al. [7] for the case of microbond testing.

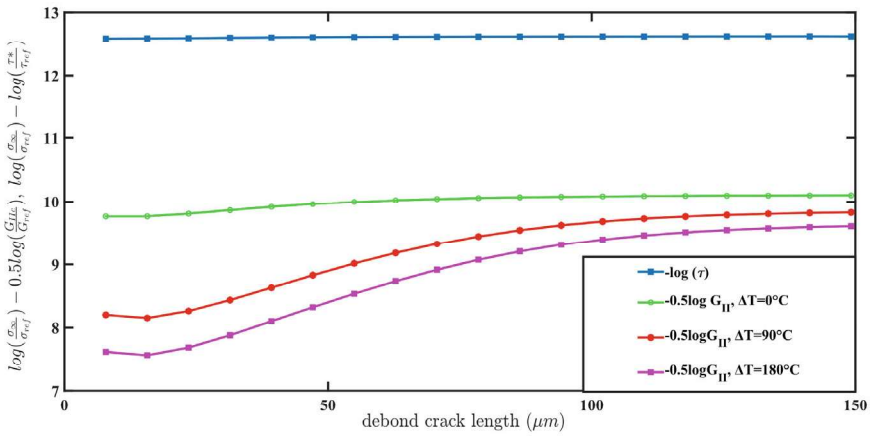


**Fig. 7** Inconsistent predictions of interfacial debond crack propagation between the energy and stress-based criteria in a hybrid composite at different residual stresses

## 4 Conclusion

Debond crack propagation in a hybrid carbon-glass–epoxy composite has been studied using finite elements based on energy released rates and a stress-based criterion. It is found that on contrary to the observation in microbond test of Zhandarov et al. [7], the predictions of the two criteria are inconsistent. The probable reasons for such differences could be (i) more complex stress state in the hybrid composite, compared to the relatively simple geometry of a pull out/microbond test; (ii) finite element model captures 3D fields. This enables a more accurate determination of energy release rate, $G_{\mathrm{II}}$ than in the 1D analytical model; (iii) the present comparison neglects the interfacial frictional stresses in the finite element calculation.

## References

1. Swolfs* Y, Gorbatikh L, Verpoest I (2014) Fibre hybridisation in polymer composites: a review. Appl Sci Manuf 67:181–200
2. Sheikh N, Mahesh S (2018) Failure mechanisms and fracture energy of hybrid materials. Int J Fract 213(1):51–81
3. Goree JG, Gross RS (1980) Analysis of a unidirectional composite containing broken fibers and matrix damage. Eng Fract Mech 13:563–578
4. Krueger R (2004) Virtual crack closure technique: history, approach, and applications. Appl Mech Rev 57(2) (American Society of Mechanical Engineers, March 2004)
5. Hedgepeth JM (1961) Stress concentrations in filamentary structures. Technical report, RN D-882, NASA
6. Liu C, Nairn J (1998) Analytical and experimental methods for a fracture mechanics interpretation of the microbond test including the effects friction and thermal stresses. Int J Adhes Adhes 19(1999):59–70

7. Zhandarov S, Pisanova E, Mäder E (2000) Is there any contradiction between the stress and energy failure criteria in micromechanical tests? Part II. Crack propagation: effect of friction on force-displacement curve. Compos Interf 7(3):149–175